Chemical Engineering Journal 480 (2024) 147908

Contents lists available at ScienceDirect

Chemical Engineering Journal

journal homepage: www.elsevier.com/locate/cej

Coupling glycerol oxidation reaction using Ni-Co foam anodes to CO_2 electroreduction in gas-phase for continuous co-valorization

Kevin Fernández-Caso [a], Martí Molera [b], Teresa Andreu [b], Jose Solla-Gullón [c], Vicente Montiel [c], Guillermo Díaz-Sainz [a,*], Manuel Álvarez-Guerra [a], Angel Irabien [a]

[a] Departamento de Ingenierías Química y Biomolecular, Universidad de Cantabria, Avda. Los Castros, s/n, 39005 Santander, Spain
[b] Facultat de Química. Departament de Ciència dels Materials i Química Física. Universitat de Barcelona / IN2UB. c/Martí i Franquès, 1, 08028 Barcelona, Spain
[c] Instituto de Electroquímica, Universidad de Alicante, Apdo. 99, E-03080 Alicante, Spain

ARTICLE INFO

Keywords:
Continuous CO_2 electroreduction
Gas-phase operation
Membrane electrode assembly
Single pass glycerol oxidation reaction
Ni-Co foam-based anodes

ABSTRACT

Electrocatalytic reduction of CO_2 is a promising alternative for storing energy and producing valuable products, such as formic acid/formate. Continuous gas-phase CO_2 electroreduction has shown great potential in producing high concentrations of formic acid or formate at the cathode while allowing the oxygen evolution or the hydrogen oxidation reactions to occur at the anode. It is advantageous to use a more relevant oxidation reaction, such as glycerol which is a plentiful by-product of current biodiesel production process. This work successfully manages to couple the glycerol oxidation reaction with continuous gas-phase CO_2 electroreduction to formate with the implementation of Ni-Co foam-based anodes. The MEA-electrolyzer developed can achieve significantly high formate concentrations of up to 359 g L^{-1} with high Faradaic efficiencies of up to 95%, while also producing dihydroxyacetone at a rate of 0.434 mmol m^{-2} s^{-1}. In comparison with existing literature, this represents an excellent trade-off between relevant figures of merit and can remarkably contribute to a future implementation of this coupled electrochemical system approach at larger scales.

1. Introduction

The electrochemical valorisation of CO_2, powered by renewable sources, presents a promising alternative to mitigate greenhouse gas emissions while generating value-added products. [1,2] Among these products, formic acid (HCOOH) or formate ($HCOO^-$) are particularly noteworthy. Both substances have diverse industrial applications, including rubber and leather manufacturing, and emerging roles as hydrogen carrier molecules (H_2) [3,4], as well as initial reagents for low-temperature fuel cells [5–7].

Considerable progress has been made in the development of CO_2 electrolysis, using batch [8,9] or semi-batch [10,11] systems. However, in order to advance these processes to an industrial scale, continuous operation is necessary. Gas-fed CO_2 electrolyzers have demonstrated exceptional performance for the production of $HCOO^-$ or HCOOH in terms of Faradaic efficiencies (FE) and energy consumptions (EC) for the target product, as well as the ability to achieve high product concentrations ([$HCOO^-$/HCOOH]) [12–20]. Moreover, gas-phase CO_2 electrolyzers do not require a liquid electrolyte at the cathode, which improves the mass transport of CO_2 [18]. This is particularly noteworthy as gas-phase CO_2 electrolyzers can produce high concentrations of the target product, which is crucial for achieving the economic and environmental sustainability of this electrochemical process [21,22], as well as satisfying the requirements of industrial applications [21,23].

Gas-phase CO_2 electrolyzers operated in a continuous mode for the production of $HCOO^-$ or HCOOH have shown promising results, with most previous studies focusing on cathode performance while overlooking the anode side. The hydrogen oxidation reaction (HOR) [12,13] has been used at the anode side; however, it is an expensive process that requires an additional step of water electrolysis upstream [17] and poses safety risks, including the potential for ignition and deflagration [24]. The oxygen evolution reaction (OER) [14–20] is an energy-intensive process that only yields oxygen as a low-value added product through water oxidation [25]. Therefore, it is important to couple the gas-phase CO_2 electrocatalytic reduction towards $HCOO^-$/HCOOH with a more relevant oxidation reaction to maximize efficiency [25].

In this context, recent research has shown that coupling the CO_2 electrochemical reduction reaction with an anodic reaction beyond OER

* Corresponding author.
E-mail address: diazsg@unican.es (G. Díaz-Sainz).

https://doi.org/10.1016/j.cej.2023.147908
Received 20 October 2023; Received in revised form 1 December 2023; Accepted 4 December 2023
Available online 7 December 2023

or HOR can be an effective strategy for improving the process by reducing cell potential and/or producing higher-value oxidized products [25–27]. Despite significant efforts to explore alternatives for relevant oxidation reactions, only a limited number of studies have successfully demonstrated the pairing of continuous CO_2 electroreduction towards $HCOO^-$/HCOOH with counter-reactions of interest [28–33]. Additional information is available in Table S1 of the Supporting Information. Among the approaches listed in Table S1, only one study has reported the gas-phase operation of the cathode, while the formaldehyde oxidation reaction occurred at the anode of a MEA-flow electrolyzer, operating at current densities of 100 mA cm^{-2} and ultra-low cell voltages of 0.86 V [33].

The coupling of glycerol oxidation reaction (GOR) with CO_2 electroreduction ($ERCO_2$) has great potential for reducing cell voltages by lowering anode potentials [26] and producing various high value-added products, such as dihydroxyacetone (DHA) [34]. Crude glycerol is obtained as a primary by-product (approximately 10 wt%) from the transesterification reaction of triglycerides with methanol or ethanol over a homogeneous basic catalyst, which is a commonly employed process in biodiesel production [35]. However, with the increasing demand for biodiesel, there will be an excess of crude glycerol, necessitating its conversion into other high-value-added products. Various glycerol chemical valorisation routes have been explored, including selective catalytic oxidation based on bio-, thermo-, electro-, photocatalytic conversion processes [36–39].

The combination of GOR with CO_2 electroreduction has demonstrated great potential for producing valuable oxidized products, such as DHA, glyceraldehyde (GLAD), glycolate (GLCA), tartronate (TAR), $HCOO^-$, among others, at the anode under alkaline conditions [40–45]. However, to date, few attempts have been made to integrate single pass GOR with continuous CO_2 reduction to $HCOO^-$ [34,46–49]. This information is compiled in Table S2 of the Supporting Information, which reports the main stacked components used in the electrochemical cell, the products detected from GOR, as well as various figures of merit, including the absolute cell voltage and the supplied current density. Guo et al.[46] and Van den Bosch et al.[47] focused on the continuous co-production of $HCOO^-$ from $ERCO_2$ and GOR in a flow reactor separated by an anion exchange and bipolar membranes, respectively. Three other studies [34,48,49] have utilized cation exchange membranes to prevent $HCOO^-$ crossover from the cathode to the anode, thereby maintaining $HCOO^-$ selectivity and preventing its re-oxidation. In our previous work [34], we paired the $ERCO_2$ to $HCOO^-$ with the single pass GOR in alkaline conditions in a 10 cm^2 flow cell, operating in a continuous mode, and with a liquid catholyte at the cathode. Subsequently, the interesting work developed by Junqueira and co-workers [48] also successfully attempted to pair the continuous $ERCO_2$ towards $HCOO^-$ to GOR in a 0.95 cm^2 flow reactor equipped with a cation exchange membrane. Lastly, Vehrenberg et al.[49] implemented a 4.5 cm^2 flow cell for the continuous co-valorization of CO_2 and glycerol into $HCOO^-$. It is important to note that these five previous studies [34,46–49] used aqueous electrolytes in the cathode compartment, resulting in low $HCOO^-$ concentrations, not exceeding 18 g L^{-1}, due to product dilution. Therefore, there are currently no precedents in the literature for employing a membrane-electrode assembly (MEA) reactor that is fed by a humidified CO_2 stream to produce highly concentrated HCOOH or $HCOO^-$ solutions at the cathode while simultaneously coupling single-pass GOR to different valuable products at the anode.

Here, we report a novel electrochemical system that efficiently catalyzes $ERCO_2$ towards $HCOO^-$ in a continuous gas-phase operation, while simultaneously conducting single step GOR at the anode to generate different C1-C3 products. Our system improves cathode performance by coupling a more relevant oxidation reaction, such as GOR, instead of HOR or OER. Through careful design of a continuous experimental setup, we assessed the joint performance of Bi Gas Diffusion Electrodes (Bi/C-GDE as cathode) and novel Ni-Co foams (as anode) [50], resulting in up to six glycerol oxidation products in the anolyte output stream. This indicates that the distribution of glycerol oxidation products can be modified and tuned to produce high value-added product, such as DHA, employing novel Ni-Co foam anodes in a MEA configuration. Furthermore, we have obtained one of the best trade-offs among $HCOO^-$ concentration, FEs, and ECs reported in literature, making our coupled electrochemical device a promising platform for efficient simultaneous CO_2 reduction and glycerol oxidation.

2. Methodology

2.1. Electrodes fabrication and characterization

In this study, carbon-supported bismuth nanoparticles (Bi/C NPs) were employed as electrocatalysts for the cathode and were shaped into a Gas Diffusion Electrode (Bi/C-GDE). The synthesis and characterization of Bi/C NPs and Bi/C-GDE were extensively described in previous studies [51]. The Bi/C-GDE consists of three layers: a carbonaceous support (Toray carbon paper, TGP-H-60), a microporous layer (MPL), and a catalytic layer (CL), as described in more detail in a previous work [51]. In brief, an MPL was air-brushed over the Toray carbon paper support, formulated with Vulcan XC-72R and PTFE (Polytetrafluoroethylene preparation, 60 wt% dispersion on H_2O, Sigma Aldrich) in a mass ratio of 40/60. The ink was then diluted in isopropanol to obtain a final slurry of 3 wt%, and sonicated for 30 min before being sprayed onto the carbon paper support using the air-brusher. After reaching a Vulcan XC-72R loading of 2 mg·cm^{-2}, both layers were sintered at 350 °C for 30 min. Subsequently, a CL was sprayed over the MPL using the same technique. The catalytic ink was composed of Bi/C NPs in Nafion (Nafion D-521 dispersion, 5 w/w % in water and 1-propanol, 0.92 meq g^{-1} exchange capacity) with a mass ratio of 70/30, which were then diluted in isopropanol and sonicated under the same conditions as described for the MPL. To ensure rigorous comparisons with previous studies, the loading of Bi/C NPs in the CL was kept at 0.75 mg cm^{-2} for the aqueous-fed reactor and increased to 1.50 mg cm^{-2} for the gas-fed MEA-reactor. As detailed in previous contributions [14,51], these Bi/C loadings were the most convenient loadings to efficiently catalyze the CO_2 reduction to $HCOO^-$ under the cathode operating conditions.

Furthermore, nickel–cobalt electrocatalysts with atomic ratios of 1:2 (Ni-Co foam) were synthetized through cathodic electrodeposition on commercially available nickel foam substrates (Recemat Ni-4753, 1.6 mm thick) to be utilized as anodes for GOR in an alkaline medium. To prepare the nickel foam substrate, it was initially pre-cleaned with 2.0 M HCl to remove native oxides. The electrodeposition process employed an aqueous electrolyte composed of 0.1 M $NaNO_3$ and 0.1 M metal precursors ($NiSO_4$·6 H_2O and $CoSO_4$·7 H_2O).

During the electrosynthesis process, the reduction of nitrate anions occurred at −1.0 V vs. Ag/AgCl (3.5 M KCl), resulting in the simultaneous precipitation of nickel and cobalt hydroxides on the substrate. The deposition technique was carried out at room temperature for 15 min using a VMP-2 Biologic multichannel potentiostat. Subsequently, the resulting materials were subjected to thermal treatment at 350 °C in air. Detailed information on the synthesis and characterization of Ni-Co foam-based anodes can be found in previous literature [50].

The morphology and the composition of the Ni-Co foam electrodes were examined using a Quanta 200 SEM equipped with an energy dispersive X-ray spectroscopy (EDS) detector. To evaluate the electroactive surface area of the Ni-Co foam anodes, electrochemical capacitance studies were performed in a standard three-electrode electrochemical glass cell. The electrolyte used was an Ar-saturated 1.0 M KOH solution. A platinum wire and a reversible hydrogen electrode (RHE) were employed as counter and reference electrodes, respectively. The experiments were carried out at ambient temperature and pressure using a PGSTAT302N system (Metrohm Autolab B. V.). For the sake of comparison, the commercial nickel foam substrate and a Pt-based particulate electrode (Pt/C-PE) [34] (with a Pt/C loading of 1.0 mg cm^{-2} and prepared by deposition of carbon-supported Pt nanoparticles (Pt/C)

(20 wt%, particle size ≤ 5 nm, Sigma Aldrich) onto a Toray carbon paper (TGP-H-60)) were also evaluated. Also, the response of the bare Toray carbon paper and a Toray carbon paper modified with Vulcan XC-72R (carbon loading of 0.8 mg cm^{-2}) were also performed to properly evaluate the contribution of the Pt nanoparticles. In all cases, portions of about 1 cm^2 (geometric area) were analysed.

2.2. Experimental setup

In this study, we used two types of electrodes, namely Bi-GDE and Ni-Co foam, which were prepared and characterized prior to their use as working (cathode) and counter (anode) electrodes, respectively. Both electrodes had a geometric surface area of 10 cm^2 and were incorporated in a continuous filter press electrochemical reactor. Initially, the experimental set-up comprised two peristaltic pumps (Watson Marlow 320, Watson Marlow Group), and a potentiostat–galvanostat (Arbin Instruments, MSTAT4) when a liquid catholyte was fed to the cathode compartment of the filter-press reactor (Fig. S1a of the Supporting Information). In this case, the catholyte employed at the cathode side consisted of a solution of 0.5 M KCl (potassium cloride, pharma grade, PanReac AppliChem) + 0.45 M $KHCO_3$ (potassium hydrogen carbonate, pharma grade, PanReac AppliChem). This aqueous-fed approach was chosen to enable a rigorous comparison between our results and those of our previous work, where we coupled GOR with Pt-based anodes [34]. Subsequently, experiments were carried out by delivering a vapour CO_2 feed to the cathode. Fig. S1b of the Supporting Information illustrates a simplified scheme of the experimental set-up employed, when the humidified CO_2 stream is supplied to the MEA-reactor. A Vapour Delivery Module (Vapour Delivery Module, Bronkhorst) was used to continuously supply the CO_2/water gas mixture (instead the peristaltic pump to drive the liquid catholyte). The humidified CO_2 stream was fed through the Bi-GDE, maintaining a molar ratio stream per mole of CO_2 and geometric area of working electrode of 0.02 mol H_2O [mol CO_2 cm^2]$^{-1}$. These cathodic operating conditions were selected according to a previous study of our research group, which used OER as anodic reaction [14]. For both experimental setups (Fig. S1a and S1b of the Supporting Information), the anolyte was composed of an aqueous solution of 1.0 M KOH (potassium hydroxide, 85% purity, pharma grade, PanReac AppliChem) + 1.0 M GLY (glycerol, 99% purity, ReagentPlus, Sigma Aldrich).

Fig. 1 illustrates the internal structure of the filter press reactor configuration with stacked components (Micro Flow Cell, ElectroCell, A/s). The cathodic and anodic compartments of the CO_2 electrolyser are separated by a Nafion 117 cation exchange membrane (Alfa Aesar) to prevent reactant mixing. A leak-free Ag/AgCl 3.5 M KCl reference electrode was positioned near the working electrode in the anodic compartment. In the case of an aqueous-fed reactor, a liquid flow distributor was placed between the cathode and the membrane to measure $HCOO^-$ in the output catholyte stream (Fig. 1a). When the reactor configuration operates in a gas-phase operation, the Bi-GDE, Nafion 117 membrane and Ni-Co foam were assembled to form the MEA-reactor (Fig. 1b).

The experiments were performed in duplicate, with a single pass of reactants through the electrochemical reactor in both the cathodic and anodic compartments, and a duration of 3600 s. The experiments were carried out under ambient conditions of pressure and temperature. Samples of catholyte and anolyte were collected every 900 s. To measure DHA and GLAD concentrations in alkaline media, the anolyte sample

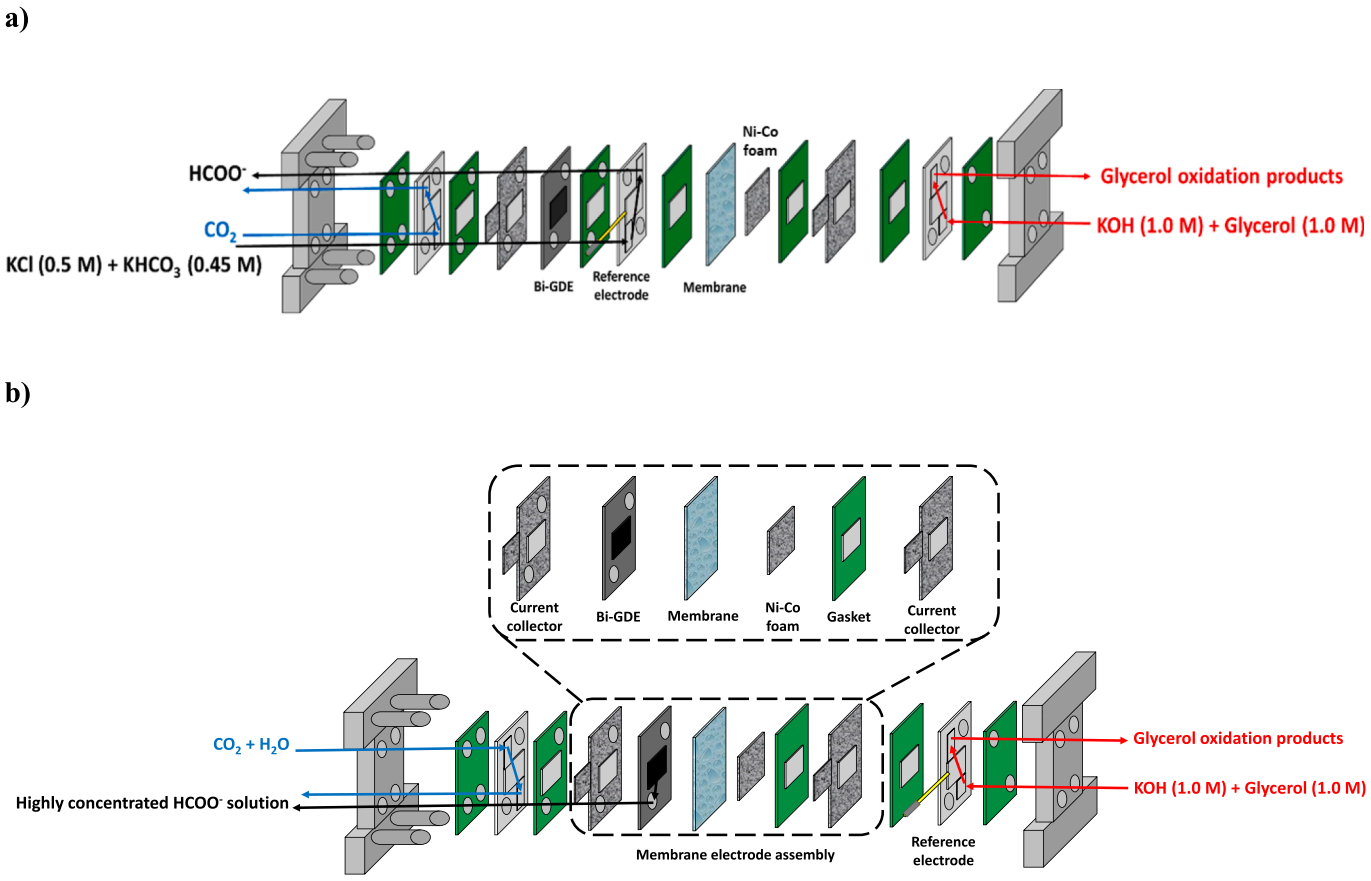

Fig. 1. Schematic illustration of CO_2 filter press reactor with stacked components, working with (from left to right) a Bi-GDE (as working electrode); a cationic exchange membrane (Nafion 117) as compartment separator; and the novel Ni-Co foam (as counter electrode), in which **a)** the catholyte flow distributor was placed between the membrane and the cathode and (aqueous-fed reactor with a liquid catholyte) **b)** both Bi-GDE, Nafion 117 and Ni-Co foam anode conform the MEA-system fed with a humidified CO_2 stream at the cathode side.

was neutralized with a 1.0 M H_2SO_4 solution (Sulfuric acid, 98% purity, pharma grade, PanReac AppliChem). Additionally, samples were collected every 15 min from the output stream at the anode side to measure the concentrations of the different glycerol oxidation products, assess glycerol conversion, and estimate the carbon balance.

2.3. Analytical techniques

Ion chromatography was employed to determine the concentration of $HCOO^-$ in the cathode outlet stream and anolyte. A Dionex ICS system equipped with an AS9 – HC column and Na_2CO_3 as the eluent was used for this purpose. The eluent was prepared at a concentration of 4.5 mM and a flowed at a of 1 mL min^{-1}.

The oxidation products of glycerol, including DHA, GLAD, TAR and GLYC, were quantified using High Performance Liquid Chromatography (HPLC) equipped with a diode array detector. An Agilent 1100 series VWD was used in combination with an ion exchange column composed of a sulfonated styrene/divinylbenzene monodisperse matrix (Hi-Plex-H, 300 × 7.7 mm, Agilent). The eluent consisted of a mixture of an aqueous phase solution of 5 mM H_2SO_4 and an organic phase of acetonitrile (Acetonitrile CHROMASOLV^{TM} Plus, for HPLC ≥ 99.9 %) at a volumetric ratio of 94/6 v/v %, respectively. The eluent flow rate was fixed at 0.6 mL·min^{-1}, and the column temperature was set at 50 °C. A constant injection volume of 50 μL was used for all samples.

The glycerol concentration in the output stream was measured using Attenuated Total Reflection (ATR, PerkinElmer) - Fourier-Transform Infrared Spectroscopy (FTIR, PerkinElmer) in the wavelength range between 1000 and 1100 cm^{-1}. The concentration of carbonates (CARB) in the form of inorganic carbon present in the output stream of the anodic compartment was determined using a total organic carbon analyser (TOC).

The average concentration value of all compounds was calculated, and figures of merit were employed to assess the overall performance of the electrochemical process. The equations for the figures of merit are reported in Equations S1-S11 of the Supplementary Information (SI).

3. Results and discussion

3.1. Electrode characterization

The characterization of the Ni-Co foam anodes previous testing was explained in more detail in a previous contribution [50]. This section will be focused on the characterization of Ni-Co foam anodes after galvanostatic tests. Fig. S2a of the Supporting Information shows the post-mortem macroscopic appearance of the Ni-Co foam anode, evidencing that the lighter grey areas are the external side of commercial nickel foam substrate. Furthermore, in the Fig. 2 it is also observed that a part of the coating has delaminated (low mechanical resistance), meanwhile the lighter areas show the nickel foam substrate. EDS mapping, detailed in the Fig. S2b of the Supporting Information, also contrast this affirmation, in which the point 2 does not present cobalt on the nickel foam surface. Thus, the mechanical properties of the Ni-Co coating should be improved to avoid erosion at the external surface by the assembly with other components or internally by the electrolyte flow at high rates. However, at the internal surface of the 1.6 mm foam electrode, the Ni-Co electrocatalyst is preserved on the nickel substrate as seen in the points 1 and 3 of the EDS spectra (Fig. S2b of Supporting Information), and the observed erosion was not considered significant. Figure S3 provides additional evidence of the coating condition. It reveals that some coatings (points 2 and 3) of the second sample of Ni-Co foam-based anode have experienced delamination. Additionally, EDS mapping shows the presence of K^+ cations from the anolyte.

3.2. $HCOO^-$ from CO_2 with a liquid catholyte: Effect of pairing GOR with Ni-Co foams anodes vs platinum particulate anodes.

Initial tests were conducted to evaluate the feasibility of using Ni-Co foam anodes in our experimental setup for GOR. In these preliminary tests, we pumped aqueous electrolyte into the cathode compartment at a specific flow rate per geometric cathode surface area (Qc/A) (0.57 and 0.15 mL min^{-1} cm^{-2}) to compare the results with our previous approaches using Pt-based particulate anodes (Pt/C-PE) [34]. The performance of these two systems was compared under the same experimental set-up and operating conditions, and the results are summarized in Table S3 of the Supporting Information. The Bi/C NPs loading at cathode

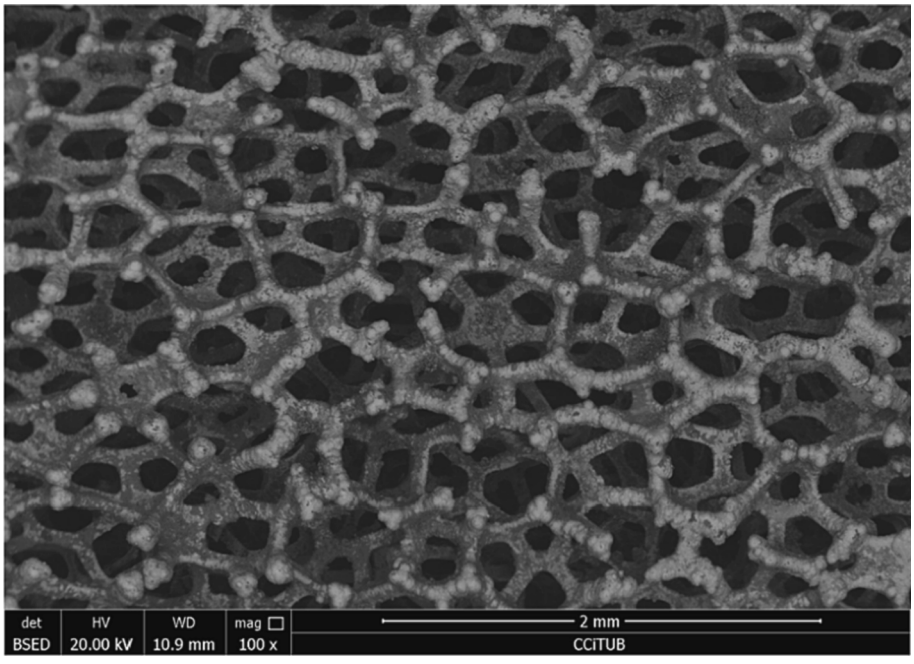

Fig. 2. SEM image of the Ni-Co foam anode employed (sample 1) after the electrolysis in galvanostatic conditions.

was fixed at 0.75 mg cm^{-2} since the best results were obtained with these loadings in our previous work with a catholyte-fed reactor [51].

Initially, we set the Qa/A of 0.57 mL min^{-1} cm^{-2} and j of 45 mA cm^{-2}, resulting in relatively low $HCOO^-$ concentrations in the catholyte of 0.72 g L^{-1}. However, this approach gives rise to a significant reduction in absolute cell voltages, from 3.46 V [34] to 2.69 V, primarily attributed to a decrease in anode potential. This significant decrease in anode potential could be related to a mere increase in the electroactive surface area of the Ni-Co foam anodes. To evaluate this question, electrochemical capacitance measurements were performed. The results are shown in Figure S4 of the Supporting Information and clearly indicate that the electroactive surface area of the Ni-Co foam anodes (in terms of capacitance) is comparable (slightly smaller) with that obtained with the Pt/C-PE but not larger. In consequence, the decrease in anode potential cannot be justified in terms of an increase in the electroactive surface area of the Ni-Co foam anodes.

Due to the reduction in absolute cell voltages, the energy consumption was slightly lower, measuring 220 kWh $kmol^{-1}$, which represents a 6 % decrease compared to Pt/C-PE-anodes (Table S3 of the Supporting Information).

Interestingly, increasing Qa/A to 2.28 mL min^{-1} cm^{-2} resulted in an increment of up to 15 % in $HCOO^-$ concentrations in the cathode (0.83 g L^{-1}) and improved FEs and production rates to 74 % and 1.74 mmol m^{-2} s^{-1}, respectively. Under these conditions, ECs of 165 kWh $kmol^{-1}$ were achieved, which almost represents a 40% reduction compared to our previous work using Pt/C-PE [34].

By adjusting the current density to 90 mA cm^{-2} and the catholyte flow rate to 0.15 mL min^{-1} cm^{-2}, similar $HCOO^-$ concentrations of approximately 7 g L^{-1} in the catholyte stream (Table S3 of the Supporting Information) were obtained with the different anodes. Similarly, comparable FEs and production rates of 83 % and 3.87 mmol m^{-2} s^{-1}, respectively, were observed. Notably, the use of Ni-Co foam anodes resulted in a significant reduction in energy consumption (approximately 27 %) compared to our previous work [34].

Table S3 of the Supporting Information also shows a further comparison with our previous studies of the research group using the same reactor configuration, Bi/C-GDE and cathode operating conditions (catholyte flow rate per geometric surface area and current density) paired with the OER. These experiments were conducted with a commercial Dimensionally Stable Anode (DSA/O_2) [DSA/O_2 (Ir-MMO (mixed metal oxide) on platinum)] [51]. In summary, the catholyte-fed reactor produced similar $HCOO^-$ concentrations at the cathode to those obtained by pairing the OER with the DSA/O_2 (Table S3 of the Supporting Information). In contrast, by working at current densities and Qc/A of 45 mA cm^{-2} and 0.57 mL min^{-1} cm^{-2}, respectively, low anode potentials were registered (1.20 V vs. Ag/AgCl), allowing to decrease the absolute cell voltage to 2.33 V respect to the value of 3.00 V obtained when the DSA/O_2 was employed to catalyze the OER. This low cell voltage value significantly reduced the ECs to 165 kWh $kmol^{-1}$, which represents a drop of almost 20 % compared with the OER-based system (Table S3 of the Supporting Information). Surprisingly, at higher current densities of 90 mA cm^{-2} and at low Qc/A of 0.15 mL min^{-1} cm^{-2}, an absolute cell voltage of 3.40 V was measured versus the value of 3.10 V attained by OER-based system, and thus increasing the ECs from to 186 to 219 kWh $kmol^{-1}$.

Another advantage of this coupled electrochemical system lies in the production of value-added oxidized products from glycerol at the anode. In summary, the main oxidized product from GOR with FEs ranging between 50 and 60 % was $HCOO^-$ (Figure S5), which was measured at modest concentrations in the anolyte stream (<0.4 g L^{-1}) as can be checked in the Figure S6. On the other hand, the FEs (Figure S5) and production rates (Figure S7) of C3 oxidized products, such as DHA or GLAD, from GOR tended to increase with higher space velocities. Nevertheless, it is important to note that higher space velocities result in lower product concentrations (Figure S6) and carbon balance (Figures S8). Detailed information about the concentrations of glycerol oxidized products in the output anolyte stream of the catholyte-fed reactor, their FEs, and production rates can be found in Tables S4-S8 of the Supporting Information. The performance of the GOR can also be evaluated using other figures of merit, such as the glycerol conversion, the carbon balance and the overall Faradaic efficiency of each test, as summarized in Table S9, indicating successful quantification of a significant portion of the glycerol oxidation products.

The use of Ni-Co foam based anodes resulted in promising results, particularly reduced cell voltages compared to our previous work with Pt/C-PE [34] and similar $HCOO^-$ production rates in the cathode, which has resulted in low ECs. In particular, by pumping a Qa/A of 2.28 mL min^{-1} cm^{-2}, interesting performances in terms of FEs and production rates were achieved, surpassing our previous approach with Pt-based anodes [34]. Nevertheless, the employment of a liquid catholyte gives rise to low $HCOO^-$ concentrations at the cathode (<7 g L^{-1}), and therefore, it is of interest to work with a humidified CO_2 stream at the cathode with the aim of achieving much higher $HCOO^-$ concentrations and closer to industrial requirements.

3.3. Gas-phase operation to increase the $HCOO^-$ concentration at the cathode

In this section, the coupling of GOR with $HCOO^-$ production at the cathode in a gas-fed MEA-reactor was evaluated and compared with previous studies on the same electrochemical system and operating conditions in which Pt/C-PE were used as anodes to catalyze GOR. Additionally, to minimize ohmic resistance and reduce cell voltages, the use of a MEA system with a Ni-Co foam anode assembled with the membrane and cathode is studied thus ensuring a sufficient wetting of the cation exchange membrane (see Fig. 1b). The integration of an MEA-system with a humidified CO_2 stream offers a promising solution for attaining significantly higher $HCOO^-$ concentrations compared to the catholyte-fed reactor setup. As previously stated, the Bi/C NPs loading at cathode was fixed at 1.50 mg cm^{-2} for all vapour-fed electrochemical tests according to a previous work [14].

Preliminary tests in gas-phase operation were conducted with Pt/C-PE (commercial carbon-supported Pt nanoparticles (20 wt% metal content) with a catalyst loading of 1.00 mg cm^{-2}) [34] as anodes to catalyze GOR, resulting in $HCOO^-$ concentrations of about 89.5 g L^{-1} at H_2O/CO_2 molar ratio and current densities of 0.02 mol H_2O [mol CO_2 $cm^2]^{-1}$ and 45 mA cm^{-2}, respectively. However, the resulting FEs and production rates for this product were 56 % and 1.32 mmol m^{-2} s^{-1}, respectively, which were lower than those obtained with Ni-Co foams-based anodes (Table 1). In addition, high absolute cell voltages of 4.95 V were recorded, which were attributed to the high anode potentials (3.73 V vs. Ag/AgCl), resulting in elevated energy consumptions of up to 467 kWh $kmol^{-1}$, representing an increase of approximately 110 % compared to the electrochemical system with Ni-Co foam-based anodes.

Table 1 also summarizes the results obtained under the same operating conditions of H_2O/CO_2 molar ratio (0.02 mol H_2O [mol CO_2 $cm^2]^{-1}$), current density (45 mA cm^{-2}), and anolyte flow rate per geometric anode surface area (Qa/A) of 0.57 mL min^{-1} cm^{-2}, using the Ni-Co foam anodes in an MEA system. The cathode potentials remained similar (-1.00 V vs. Ag/AgCl), while the anode potential was slightly more positive (2.29 V vs. Ag/AgCl) than that obtained by pairing the OER (2.00 V vs. Ag/AgCl) [14] under the same conditions (see Table 1). $HCOO^-$ concentrations of up to 172 g L^{-1} were obtained with promising values of the different figures of merit used to assess cathode performance. The FEs and production rates towards this target product were approximately 80 % and 1.86 mmol m^{-2} s^{-1}, respectively. However, despite achieving lower $HCOO^-$ concentrations measured and a slightly higher absolute cell voltage of 3.29 V, the EC was adversely affected, with a value of 221 kWh $kmol^{-1}$.This was nearly 17 % higher than the value obtained with the OER-based system (189 kWh $kmol^{-1}$) [14].

The results obtained with the catholyte-fed reactor (see section 3.2.) indicated that by increasing Qa/A to 2.28 mL min^{-1} cm^{-2} $HCOO^-$

Table 1
Bi/C-GDE (with catalyst loading of 1.50 mg cm^{-2}) performance in the $HCOO^-$ production in the gas-fed MEA reactor system by working with at a H_2O/CO_2 molar ratio per geometric surface area and a current density of 0.02 molH_2O [molCO_2 cm^2]$^{-1}$ and 45 mA cm^{-2}, respectively, taking into account (i) the counter electrode and the oxidation reaction of the anode which can be glycerol (GOR) which can be catalyzed by the Pt/C-PE (preliminary tests) or the Ni-Co foam (this work); or water oxidation (OER) boosted by DSA/O_2[14]; (ii) the anolyte flow rate per geometric anode surface area [Qa/A]; (iii) the absolute cell voltage; (iv) the anode potential; (v) the cathode potential; (vi) the $HCOO^-$ concentration [$HCOO^-$]; (vii) the Faradaic efficiency [FE] towards $HCOO^-$; (viii) the production rate of $HCOO^-$ [r$HCOO^-$]; (ix) the energy consumption per kmol of $HCOO^-$ [EC]; and (x) the standard deviation.

Counter-electrode	Qa/A (mL min^{-1} cm^{-2})	Absolute cell voltage (V)	Anode potential (V)	Cathode potential (V)	[$HCOO^-$] (g L^{-1})	FE for $HCOO^-$ (%)	r_{HCOO^-} (mmol m^{-2} s^{-1})	EC (kWh $kmol^{-1}$)	Standard deviation (%)
Pt/C-PE - GOR	0.57	4.95	3.73	−1.22	89.5	56.1	1.32	467	0.79
Ni-Co foam - GOR		3.29	2.29	−1.00	172.5	79.9	1.86	221	3.18
Pt/C-PE - GOR	2.28	5.06	3.75	−1.31	77.4	39.9	0.92	700	2.89
Ni-Co foam - GOR		3.40	2.39	−1.01	359.5	95.1	2.21	192	0.98
DSA/O_2 - OER	0.57	3.00	2.00	−1.00	337.0	89.1	2.08	189	3.44

concentrations can be improved at the cathode, thereby improving the figures of merit analyzed [52]. This improvement may be attributed to an optimized balance between membrane hydration and potassium availability near the catalyst surface, which facilitates the collection of concentrated $HCOO^-$ directly from the cathodic stream [16].

By also increasing Qa/A from 0.57 to 2.28 mL min^{-1} cm^{-2} in gas-phase operation, a relevant improvement of the figures of merit associated with $HCOO^-$ production at the cathode were observed. Concentrated $HCOO^-$ solutions of up to 359 g L^{-1} (>30 wt%) were produced with high FEs of 95 % and promising ECs of 192 kWh $kmol^{-1}$. These are outstanding numbers that evidence that the coupled electrochemical device can achieve comparable $HCOO^-$ production to previous approaches paired with the OER and using the same experimental set-up [14].

3.4. Analysis of the effect of the anolyte flow rate on the glycerol oxidation products distribution coupled with the gas-phase operation in the cathode

This section focuses on evaluating the distribution of glycerol oxidation products, production rates and FEs of detected products in the anolyte output stream (calculated using Equations S1-S11 from the Supporting Information) during the gas-phase CO_2 reduction reaction to $HCOO^-$ at the cathode (section 3.3). Fig. 3 presents an assessment of the FEs (3a) and production rates (3b) of the main products detected from GOR in the anolyte output stream of the MEA reactor for different Qa/A values of 0.57 and 2.28 mL min^{-1} cm^{-2}, respectively, for easy comprehension.

Initial experiments were conducted under the same operating conditions as previous studies [14], including an anolyte flow rate per geometric anode surface area of 0.57 mL min^{-1} cm^{-2}, a current density of 45 mA cm^{-2}, and a H_2O/CO_2 molar ratio per geometric cathode surface area of 0.02 mol H_2O [mol CO_2 cm^2]$^{-1}$. $HCOO^-$ was the primary product obtained from GOR under the above specific operating conditions, with an interesting FE of up to 48.62 % and a production rate of 850μ mol m^{-2} s^{-1}. In addition, the production of C2 products, such as GLYC, was quantified with FEs and production rates of 13.91 % and 180.68μ mol m^{-2} s^{-1} respectively. At the given current densities, CARB, the most oxidized product, was obtained with a FE and production rate of up to 11.12 % and 110.50μ mol m^{-2} s^{-1}, respectively. Promising FEs and production rates were also achieved for 3 carbon products such as GLAD (7.37 % and 172.04μ mol m^{-2} s^{-1}) and TAR (1.52 % and 8.80μ mol m^{-2} s^{-1}), respectively. Finally, under alkaline conditions, a high value-added product such as DHA, was produced with FE and production rate of 4.23 % and 98.83μ mol m^{-2} s^{-1}, respectively. Table S10 in the Supporting Information provides detailed information on the FEs and production rates of each product detected from GOR.

A comprehensive analysis of the oxidation products and carbon balance of 2 %, with an overall FE of 86 % (Table S10 in the Supporting Information) was conducted. This implies that most of the products from GOR were successfully detected. The remaining FE could be attributed to trace amounts of gaseous products, such as CO_2 generated from GOR, and/or the more competitive and reactive OER, which may have been influenced by the high concentration of KOH in the anolyte [53,54].

Although some products, such as DHA, are well-known to be unstable in alkaline conditions [44], reducing the residence time of DHA in this medium, before neutralization with 1.0 M H_2SO_4, that is, by simply operating at higher anolyte flow rates per geometric anode surface area, was shown to be a convenient alternative [34]. To get further insights on this, an additional test was conducted anolyte flow rates per geometric anode surface area of 2.28 mL min^{-1} cm^{-2}. Under these anode conditions, the FEs towards $HCOO^-$ decreased to 34.82 %, while the formation of CARB with an FE of 21.57 % increased, as shown in Fig. 3a. The production rates of $HCOO^-$ and CARB were also affected, with values of 609μ mol m^{-2} s^{-1} and 215μ mol m^{-2} s^{-1}, respectively. This could be attributed to CARB being formed from further oxidation of $HCOO^-$ anion over the catalyst surface, which may explain the reduction in FE and production rate of $HCOO^-$ for this Qa/A value [55]. At an anolyte flow rate per geometric anode surface area of 2.28 mL min^{-1} cm^{-2}, GLYC was not detected in the anode side, possibly because GLYC is correlated with the re-oxidation of GLYAC anion, which comes from the GLAD reaction pathway (Fig. 3c). Similarly, TAR was also not detected in the anolyte output stream of the filter press reactor, and its detection was associated with the same reaction pathway as the GLYC anion. In contrast, there was a slight increase in the FEs and production rates of GLAD, which were 8.8 % and 205.34μ mol m^{-2} s^{-1}, respectively. This increase may be attributed to the low residence time of GLAD, resulting in lower re-oxidation of this compound into other more oxidized compounds such as GLYC, TAR or $HCOO^-$ (Fig. 3c).

Lastly, Figure S9 of the Supporting Information also shows that all oxidation products had lower concentrations by increasing Qa/A from 0.57 to 2.28 mL min^{-1} cm^{-2}, except for DHA concentration, which slightly increased from 94 to 103 mg L^{-1}. The FEs and rates for DHA were increased from 4.23 % and 98.83μ mol m^{-2} s^{-1}, respectively, to 18.62 % and 434μ mol m^{-2} s^{-1}, respectively, indicating that higher amounts of this relevant product can be obtained in alkaline conditions by controlling the anolyte flow rate pumped to the filter press reactor.

3.5. Pairing GOR to $ERCO_2$ as pathway to improve trade-offs in the figures of merit

Numerous recent studies have explored the electrocatalytic reduction of CO_2 to $HCOO^-$ or HCOOH in continuous gas-phase operation, many of them reporting notable performances (Fig. 4) [12–20]. These

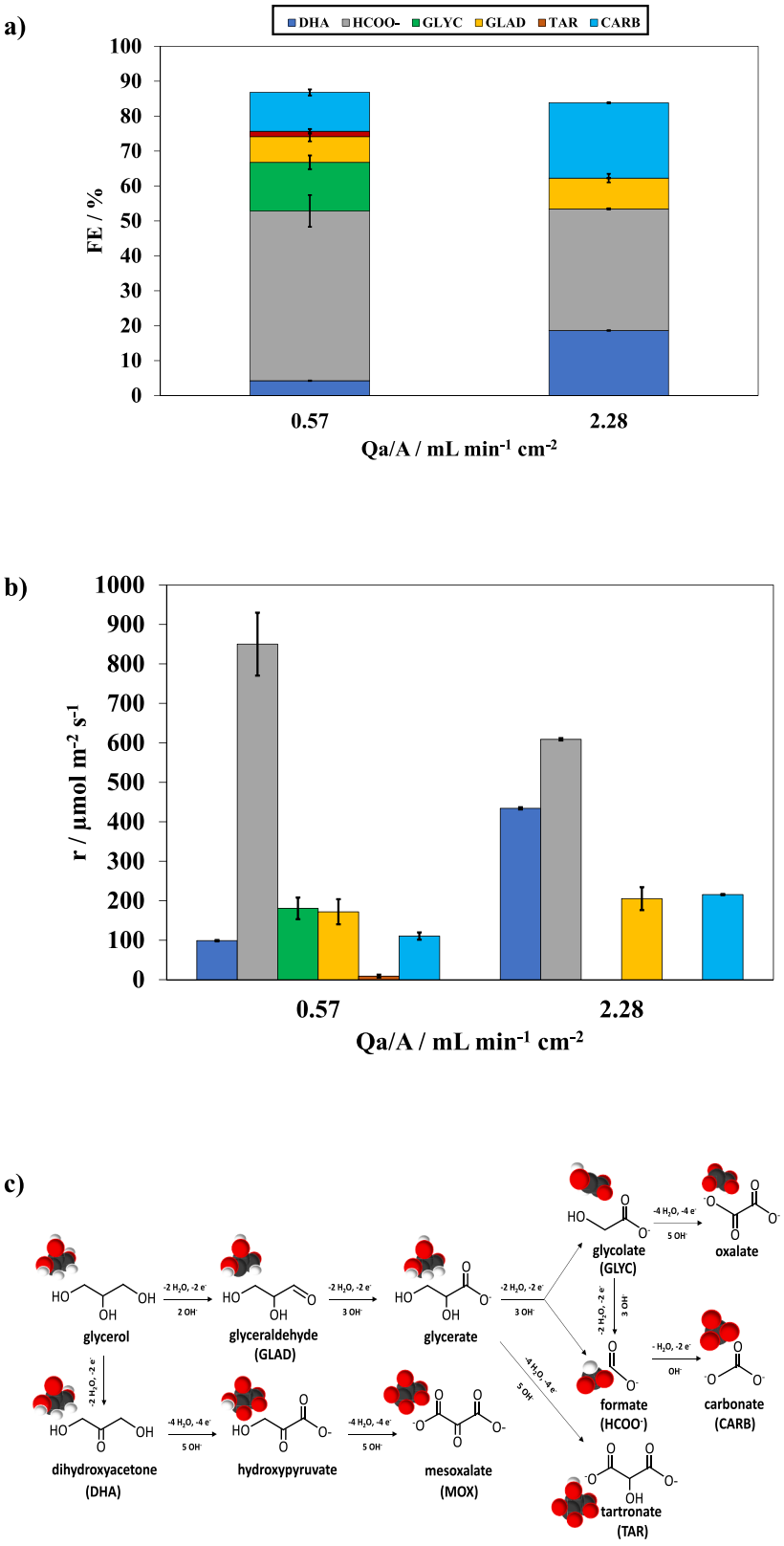

Fig. 3. a) Faradaic Efficiencies [FE] and b) production rates [r] of the different detected products from GOR in the gas-phase MEA reactor as a function of the anolyte flow rate per geometric anode surface area (Qa/A) with a single-pass operation though the anode compartment at fixed values of the H_2O/CO_2 molar ratio per geometric cathode surface area and the current densities of 0.02 mol H_2O [mol CO_2 $cm^2]^{-1}$ and 45 mA·cm^{-2}, respectively. c) Possible reaction pathways for the electrochemical oxidation of glycerol to various value-added products in alkaline medium. Adapted from ref.[43].

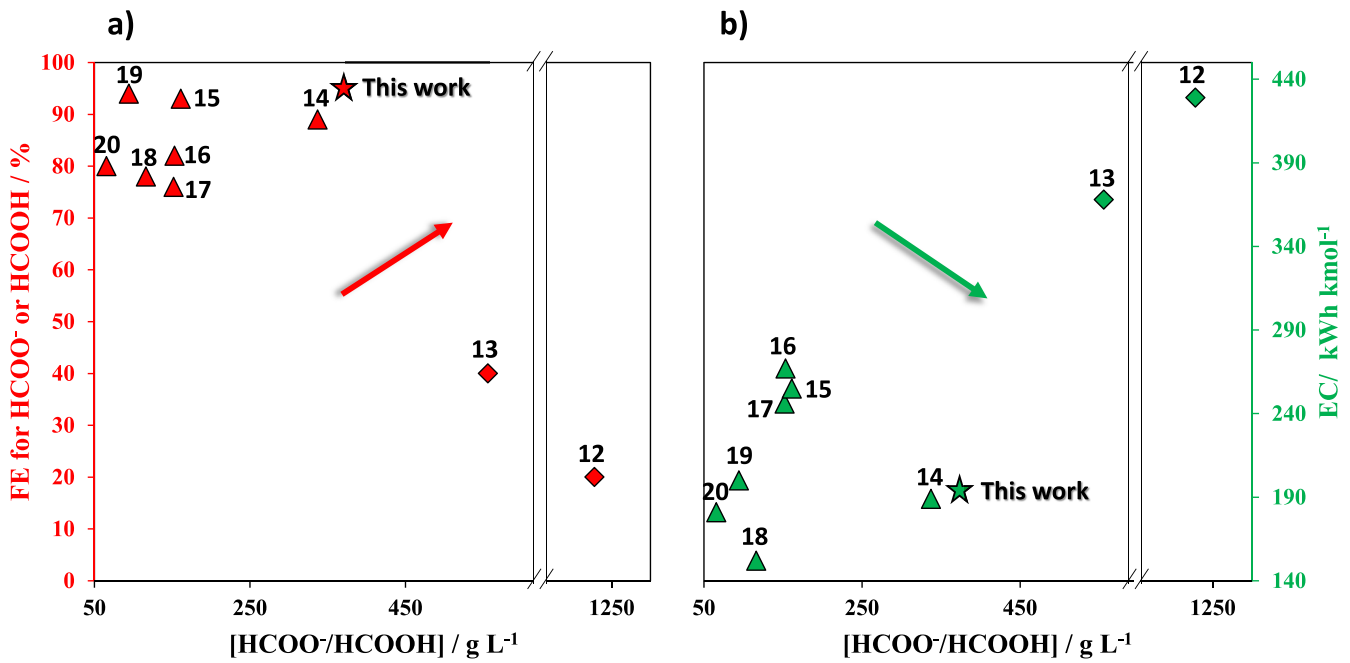

Fig. 4. Current state of the art for the continuous gas-phase CO_2 electrocatalytic reduction to HCOOH or $HCOO^-$ in terms of two figures of merit: **a)** the Faradaic efficiency of $HCOO^-$/HCOOH [FE] (represented by red filled symbols); and **b)** the energy consumptions per kmol of $HCOO^-$ or HCOOH [EC] (represented by green filled symbols) as a function of the target product concentration [$HCOO^-$/HCOOH]. The studies represented by diamond shapes (◆ ◆) have employed the HOR as the oxidation reaction (refs. 12 and 13); whereas the references with triangles shapes (▲ ▲) have employed the OER as the oxidation reaction (refs. 14, 15, 16, 17, 18, 19 and 20). The star symbol (★ ★) represents the data obtained in this study, which has developed the GOR at the anode.

findings bring us closer to realizing larger scale applications of this process. For instance, Fan et al.[12] and Xia et al.[13] reported HCOOH concentrations of about 500 g L^{-1} using a three-compartment reactor, with FEs towards the target product not exceeding 40 %, while the HOR takes place on the anode surface (Fig. 4a). Fig. 4b shows that these approaches with three-compartment reactors achieved ECs above 350 kWh per kmol of HCOOH (equivalent to 7.60 kWh kg^{-1}). In contrast, all other references included in Fig. 4 used the OER at the anode and reached excellent results in terms of the different figures of merit analysed.

Díaz-Sainz et al.[14] obtained one of the best trade-offs between the figures of merit with $HCOO^-$ concentrations, FEs and ECs of 337 g L^{-1}, 89 % and 180 kWh $kmol^{-1}$, respectively, at current densities of 45 mA cm^{-2}. Lin and co-workers [15] obtained HCOOH concentrations of up to 161 g L^{-1} with interesting FE towards this product and EC of 93% and 255 kWh $kmol^{-1}$, respectively, by pairing the OER at the anode in acidic conditions with an 0.5 M H_2SO_4 solution. Li et al. [16] achieved promising $HCOO^-$ concentrations of 153 g L^{-1} with FEs and ECs at 80 % and 267 kWh per kmol of $HCOO^-$, respectively, using a two-compartment reactor. Similarly, Yang et al. [17] obtained HCOOH concentrations of up to 151.8 g L^{-1} with FEs and ECs for this product of 76 % and 246 kWh $kmol^{-1}$, respectively, by implementing a three-compartment reactor. Lee and co-workers [18] achieved promising $HCOO^-$ concentrations of 116 g L^{-1} with ECs of only 152 kWh per kmol of target product by employing the cationic exchange membrane as the electrocatalyst support. Another approach conducted by Yang et al. [19], with a three compartment reactor, obtained HCOOH concentrations of 94 g L^{-1} at promising FEs towards this product and ECs of 94 % and 200 kWh $kmol^{-1}$, respectively. Finally, De Mot et al. [20] obtained $HCOO^-$ concentrations of 65.4 g L^{-1} with FEs of up to 80 % at ECs of 181 kWh $kmol^{-1}$. More information about these approaches, as well as other parameters of interest, are detailed in the Table S11 of the Supporting Information.

Among the different approaches reported in the literature, only the one by Fan et al. [12] meets the concentration requirements for HCOOH (>85 wt% or 1020 g L^{-1} which is the most common product concentration in the market [56,57]), albeit with low FEs of 20% towards this product and EC up to 429 kWh $kmol^{-1}$ (corresponding to 9.32 kWh kg^{-1}). Two other approaches [13,14] achieve target product concentrations higher than 21 wt% [21,23], and only one [14] of them demonstrates both high product concentrations and promising FEs and ECs for these products by pairing the OER at the anode. Nevertheless, none of these works manages to pair a more relevant oxidation reaction than HOR or OER at the anode side. Despite several challenges to becoming commercially viable, the electrochemical production of $HCOO^-$ or HCOOH from CO_2 shows promise [23]. Recent literature has documented remarkable results, and in particular, the present work achieves high product concentrations (359 g L^{-1}), excellent FEs (95%), and low EC (192 kWh $kmol^{-1}$). These findings represent an interesting trade-off in the continuous gas-phase CO_2 electrocatalytic reduction to $HCOO^-$/HCOOH. Furthermore, what sets this approach apart is its ability to reach this milestone by coupling a more relevant oxidation reaction, namely GOR, rather than OER or HOR.

4. Concluding remarks

The recent literature on continuous electrochemical production of $HCOO^-$ or HCOOH from CO_2 has focused on developing gas diffusion electrodes that acts as working electrodes, which are more active and stable. One of the main challenges in this process is overcoming the mass transport limitations of CO_2, which can be achieved by feeding a humidified CO_2 stream at the cathode side. On the other hand, all approaches that have demonstrated notable performances in terms of target product concentrations in continuous gas-phase electrocatalytic CO_2 conversion to $HCOO^-$ or HCOOH have employed the OER at the anode, resulting in a significant portion of the supplied energy being wasted on the production of a low value-added product, such as O_2. Other studies have explored the utilization of the HOR at the anode of three-compartment electrochemical reactors to facilitate proton release and thereby reducing operating cell voltages. Nevertheless, it is important to consider that the cost associated with H_2 feed may pose a significant economic penalty for such processes. In this sense, the utilization of single-pass operation, along with the introduction of

innovative Ni-Co foam-based anodes as demonstrated in this research, offers the opportunity to achieve high value-added products through GOR. In this study, by fixing the H_2O/CO_2 molar ratio per unit of cathode geometric surface area to 0.02 mol H_2O [mol CO_2 cm^2]$^{-1}$, promising $HCOO^-$ concentrations and FEs towards this product of 359 g L^{-1} and 95 % were achieved at the cathode output stream, respectively. Furthermore, interesting ECs of up 192 kWh per kmol of $HCOO^-$ were also obtained under these conditions, which represents one of the best trade-offs in the figures of merit analyzed. The reduced electrode spacing of the MEA allows for lower ohmic resistance, leading to decreased cell voltages and higher concentrations of $HCOO^-$ and lesser-oxidized products of high-value added by reducing the anodic potentials. Interestingly, encouraging DHA productions in alkaline conditions were achieved with FEs and production rates for this product of up to 19 % and 0.437 mmol m^{-2} s^{-1}, respectively, at anolyte flow rates per geometric anode surface area of 2.28 mL min^{-1} cm^{-2}.

While these results are promising, future approaches should be explored in order to increase the concentration of glycerol oxidation products such as DHA in the anolyte outlet stream. This will help reduce the energy costs associated with purification of this product. Furthermore, at the same time, for the practical implementation of this coupled electrochemical system, operation at relevant current densities ($\geq$200 mA cm^{-2}) must be achieved without compromising the related figures of merit. Future research should also include stability tests conducted at these relevant current densities, focussing on improving the long-term performance of the Bi/C-GDE.

CRediT authorship contribution statement

Kevin Fernández-Caso: Conceptualization, Data curation, Investigation, Methodology, Validation, Writing – original draft. **Martí Molera:** Investigation, Methodology, Validation. **Teresa Andreu:** Funding acquisition, Project administration, Supervision, Writing – review & editing. **Jose Solla-Gullón:** Funding acquisition, Project administration, Supervision, Writing – review & editing. **Vicente Montiel:** Funding acquisition, Project administration, Supervision, Writing – review & editing. **Guillermo Díaz-Sainz:** Conceptualization, Data curation, Investigation, Methodology, Supervision, Writing – original draft, Writing – review & editing. **Manuel Álvarez-Guerra:** Conceptualization, Funding acquisition, Methodology, Project administration, Supervision, Writing – original draft, Writing – review & editing. **Angel Irabien:** Funding acquisition, Project administration, Supervision, Writing – review & editing.

Declaration of Competing Interest

The authors declare that they have no known competing financial interests or personal relationships that could have appeared to influence the work reported in this paper.

Data availability

No data was used for the research described in the article.

Acknowledgements

The authors gratefully acknowledge financial support through projects PID2019-108136RB-C31, PID2019-108136RB-C32 and PID2019-108136RB-C33, PID2020-112845RB-I00, TED2021–129810B-C21 and PLEC2022-009398 (MCIN/AEI/10.13039/501100011033 and Unión Europea Next GenerationEU/PRTR). This project has received funding from the European Union's Horizon Europe research and innovation programme under grant agreement No 101118265.

Appendix A. Supplementary data

Supplementary data to this article can be found online at https://doi.org/10.1016/j.cej.2023.147908.

References

[1] W. Da Silva Freitas, A. D'Epifanio, B. Mecheri, Electrocatalytic CO2 reduction on nanostructured metal-based materials: Challenges and constraints for a sustainable pathway to decarbonization, J. CO_2 Util. 50 (2021), 101579, https://doi.org/10.1016/j.jcou.2021.101579.

[2] S. Garg, M. Li, A.Z. Weber, L. Ge, L. Li, V. Rudolph, G. Wang, T.E. Rufford, Advances and challenges in electrochemical CO_2 reduction processes: an engineering and design perspective looking beyond new catalyst materials, J. Mater. Chem. A. 8 (2020) 1511–1544, https://doi.org/10.1039/c9ta13298h.

[3] S. Chatterjee, I. Dutta, Y. Lum, Z. Lai, K.W. Huang, Enabling storage and utilization of low-carbon electricity: power to formic acid, Energy Environ. Sci. 14 (2021) 1194–1246, https://doi.org/10.1039/d0ee03011b.

[4] J. Rg Eppinger, K.-W. Huang, Formic acid as a hydrogen energy carrier, ACS Energy Lett. 2 (2022) 188–195, https://doi.org/10.1021/acsenergylett.6b00574.

[5] Z. Fang, Z. Zhang, S. Ligani Fereja, J. Guo, X. Tong, Y. Zheng, R. Liu, X. Liang, L. Zhang, Z. Li, W. Chen, Highly dispersed 1 nm PtPd bimetallic clusters for formic acid electrooxidation through a CO-free mechanism, J. Energy Chem. 78 (2023) 554–564, https://doi.org/10.1016/j.jechem.2022.12.018.

[6] H. Cheng, J. Zhou, H. Xie, S. Zhang, J. Zhang, S. Sun, P. Luo, M. Lin, S. Wang, Z. Pan, J. Wang, X.J. Loh, Z. Liu, Hydrogen intercalation-induced crystallization of ternary PdNiP alloy nanoparticles for direct formic acid fuel cells, 1–7, Adv. Energy Mater. (2023), 2203893, https://doi.org/10.1002/aenm.202203893.

[7] J. Kim, H. Kim, S. Kim, J.H. Jang, H. Sohn, S.J. Hong, J. Kim, G.H. Han, S. Choe, Y. E. Sung, S.Y. Kim, H.W. Jang, T.H. Jo, H.K. Lim, S.J. Yoo, S.H. Ahn, Atomic Pt clusters on Au dendrite for formic acid oxidation, Chem. Eng. J. 451 (2023), 138664, https://doi.org/10.1016/j.cej.2022.138664.

[8] B. Ávila-Bolívar, R. Cepitis, M. Alam, J.M. Assafrei, K. Ping, J. Aruväli, A. Kikas, V. Kisand, S. Vlassov, M. Käärik, J. Leis, V. Ivaništšev, P. Starkov, V. Montiel, J. Solla-Gullón, N. Kongi, CO_2 reduction to formate on an affordable bismuth metal-organic framework based catalyst, J. CO_2 Util. 59 (2022), 101937, https://doi.org/10.1016/J.JCOU.2022.101937.

[9] B. Ávila-Bolívar, V. Montiel, J. Solla-Gullón, On the activity and stability of Sb2O3/Sb nanoparticles for the electroreduction of CO_2 toward formate, J. Electroanal. Chem. 895 (2021), 115440, https://doi.org/10.1016/J.JELECHEM.2021.115440.

[10] A. Löwe, C. Rieg, T. Hierlemann, N. Salas, D. Kopljar, N. Wagner, E. Klemm, Influence of temperature on the performance of gas diffusion electrodes in the CO_2 reduction reaction, ChemElectroChem 6 (2019) 4497–4506, https://doi.org/10.1002/celc.201900872.

[11] A. Löwe, M. Schmidt, F. Bienen, D. Kopljar, N. Wagner, E. Klemm, Optimizing reaction conditions and gas diffusion electrodes applied in the CO_2 reduction reaction to formate to reach current densities up to 1.8 A cm^{-2}, ACS Sustain Chem. Eng. 9 (2021) 4213–4223, https://doi.org/10.1021/acssuschemeng.1c00199.

[12] L. Fan, C. Xia, P. Zhu, Y. Lu, H. Wang, Electrochemical CO_2 reduction to high-concentration pure formic acid solutions in an all-solid-state reactor, Nat. Commun. 11 (2020) 3633, https://doi.org/10.1038/s41467-020-17403-1.

[13] C. Xia, P. Zhu, Q. Jiang, Y. Pan, W. Liang, E. Stavitsk, H.N. Alshareef, H. Wang, Continuous production of pure liquid fuel solutions via electrocatalytic CO_2 reduction using solid-electrolyte devices, Nat. Energy. 4 (2019) 776–785, https://doi.org/10.1038/s41560-019-0451-x.

[14] G. Díaz-Sainz, M. Alvarez-Guerra, B. Ávila-Bolívar, J. Solla-Gullón, V. Montiel, A. Irabien, Improving trade-offs in the figures of merit of gas-phase single-pass continuous CO_2 electrocatalytic reduction to formate, Chem. Eng. J. 405 (2021), 126965, https://doi.org/10.1016/j.cej.2020.126965.

[15] L. Lin, X. He, X.G. Zhang, W. Ma, B. Zhang, D. Wei, S. Xie, Q. Zhang, X. Yi, Y. Wang, A nanocomposite of bismuth clusters and $Bi_2O_2CO_3$ sheets for highly efficient electrocatalytic reduction of CO_2 to formate, Angew. Chemie - Int. Ed. 62 (2023), e202214959, https://doi.org/10.1002/anie.202214959.

[16] L. Li, A. Ozden, S. Guo, F. Pelayo García de Arquer, C. Wang, M. Zhang, J. Zhang, H. Jiang, W. Wang, H. Dong, D. Sinton, E.H. Sargent, M. Zhong, Stable, active CO_2 reduction to formate via redox-modulated stabilization of active sites, Nat. Commun. 12 (2021) 5223, https://doi.org/10.1038/s41467-021-25573-9.

[17] H. Yang, J.J. Kaczur, S.D. Sajjad, R.I. Masel, Performance and long-term stability of CO2 conversion to formic acid using a three-compartment electrolyzer design, J. CO_2 Util. 42 (2020), 101349, https://doi.org/10.1016/j.jcou.2020.101349.

[18] W. Lee, Y.E. Kim, M.H. Youn, S.K. Jeong, K.T. Park, Catholyte-free electrocatalytic CO_2 reduction to formate, Angew. Chemie - Int. Ed. 130 (2018) 6999–7003, https://doi.org/10.1002/ange.201803501.

[19] H. Yang, J.J. Kaczur, S.D. Sajjad, R.I. Masel, Electrochemical conversion of CO_2 to formic acid utilizing SustainionTM membranes, J. CO_2 Util. 20 (2017) 208–217, https://doi.org/10.1016/j.jcou.2017.04.011.

[20] B. De Mot, M. Ramdin, J. Hereijgers, T.J.H. Vlugt, T. Breugelmans, Direct water injection in catholyte-free zero-gap carbon dioxide electrolyzers, ChemElectroChem 7 (2020) 3839–3843, https://doi.org/10.1002/celc.202000961.

[21] M. Rumayor, A. Dominguez-Ramos, A. Irabien, Environmental and economic assessment of the formic acid electrochemical manufacture using carbon dioxide: influence of the electrode lifetime, Sustain. Prod. Consum. 18 (2019) 72–82, https://doi.org/10.1016/J.SPC.2018.12.002.

[22] M. Rumayor, A. Dominguez-Ramos, P. Perez, A. Irabien, A techno-economic evaluation approach to the electrochemical reduction of CO_2 for formic acid manufacture, J. CO_2 Util. 34 (2019) 490–499, https://doi.org/10.1016/j.jcou.2019.07.024.
[23] K. Fernández-Caso, G. Díaz-Sainz, M. Alvarez-Guerra, A. Irabien, Electroreduction of CO_2: advances in the continuous production of formic acid and formate, ACS Energy Lett. 8 (2023) 1992–2024, https://doi.org/10.1021/acsenergylett.3c00489.
[24] D.A. Crowl, Y. Do Jo, The hazards and risks of hydrogen, J. Loss Prev. Process Ind. 20 (2007) 158–164, https://doi.org/10.1016/j.jlp.2007.02.002.
[25] J. Na, B. Seo, J. Kim, C. Woo Lee, H. Lee, Y. Jeong Hwang, B. Koun Min, D. Ki Lee, H.-S. Oh, U. Lee, General technoeconomic analysis for electrochemical coproduction coupling carbon dioxide reduction with organic oxidation, Nat. Commun. 10 (2019) 5193, https://doi.org/10.1038/s41467-019-12744-y.
[26] S. Verma, S. Lu, P.J.A. Kenis, Co-electrolysis of CO_2 and glycerol as a pathway to carbon chemicals with improved technoeconomics due to low electricity consumption, Nat. Energy. 4 (2019) 466–474, https://doi.org/10.1038/s41560-019-0374-6.
[27] M. Rumayor, A. Domínguez-Ramos, Á. Irabien, Feasibility analysis of a CO_2 recycling plant for the decarbonization of formate and dihydroxyacetone production, Green Chem. 23 (2021) 4840–4851, https://doi.org/10.1039/D1GC01042E.
[28] Q. Wang, X. Wang, C. Wu, Y. Cheng, Q. Sun, H. Yu, Enhanced electroreduction of CO_2 and simultaneous degradation of organic pollutants using a Sn-based carbon nanotubes/carbon black hybrid gas diffusion cathode, J. CO_2 Util. 26 (2018) 425–433, https://doi.org/10.1016/J.JCOU.2018.05.027.
[29] D. Wu, J. Hao, Z. Song, X.Z. Fu, J.L. Luo, All roads lead to Rome: An energy-saving integrated electrocatalytic CO_2 reduction system for concurrent value-added formate production, Chem. Eng. J. 412 (2021), 127893, https://doi.org/10.1016/j.cej.2020.127893.
[30] Y. Zhang, J. Lan, F. Xie, M. Peng, J. Liu, T.-S. Chan, Y. Tan, Aligned InS nanorods for efficient electrocatalytic carbon dioxide reduction, ACS Appl. Mater. Interfaces. 14 (2022) 25257–25266, https://doi.org/10.1021/acsami.2c01152.
[31] Y. Zhang, Y. Chen, R. Liu, X. Wang, H. Liu, Y. Zhu, Q. Qian, Y. Feng, M. Cheng, G. Zhang, Oxygen vacancy stabilized $Bi_2O_2CO_3$ nanosheet for CO_2 electroreduction at low overpotential enables energy efficient CO-production of formate, InfoMat. (2022) 1–12, https://doi.org/10.1002/inf2.12375.
[32] C. Xiao, L. Cheng, Y. Wang, J. Liu, R. Chen, H. Jiang, Y. Li, C. Li, Low full-cell voltage driven high-current-density selective paired formate electrosynthesis, J. Mater. Chem. A. 10 (2022) 1329–1335, https://doi.org/10.1039/d1ta08303a.
[33] M. Li, T. Wang, W. Zhao, S. Wang, Y. Zou, A pair-electrosynthesis for formate at ultra-low voltage via coupling of CO_2 reduction and formaldehyde oxidation, Nano-Micro Lett. 14 (2022) 1–17, https://doi.org/10.1007/s40820-022-00953-y.
[34] K. Fernández-Caso, A. Peña-Rodríguez, J. Solla-Gullón, V. Montiel, G. Díaz-Sainz, M. Alvarez-Guerra, A. Irabien, Continuous carbon dioxide electroreduction to formate coupled with the single-pass glycerol oxidation to high value-added products, J. CO_2 Util. 70 (2023), 102431, https://doi.org/10.1016/j.jcou.2023.102431.
[35] P.M. Walgode, L.C.D. Coelho, R.P.V. Faria, A.E. Rodrigues, Dihydroxyacetone production: from glycerol catalytic oxidation with commercial catalysts to chromatographic separation, Ind. Eng. Chem. Res. 60 (2021) 10551–10565, https://doi.org/10.1021/acs.iecr.1c00275.
[36] H. Habe, T. Fukuoka, D. Kitamoto, K. Sakaki, Biotechnological production of D-glyceric acid and its application, Appl. Microbiol. Biotechnol. 84 (2009) 445–452, https://doi.org/10.1007/s00253-009-2124-3.
[37] X. Zhang, G. Cui, H. Feng, L. Chen, H. Wang, B. Wang, X. Zhang, L. Zheng, H. Song, M. Wei, Platinum-copper single atom alloy catalysts with high performance towards glycerol hydrogenolysis, Nat. Commun. 10 (2019) 5812, https://doi.org/10.1038/s41467-019-13685-2.
[38] C. Liu, M. Hirohara, T. Maekawa, R. Chang, T. Hayashi, C.Y. Chiang, Selective electro-oxidation of glycerol to dihydroxyacetone by a non-precious electrocatalyst – CuO, Appl. Catal. B Environ. 265 (2020), 118543, https://doi.org/10.1016/J.APCATB.2019.118543.
[39] D. Liu, J.-C. Liu, W. Cai, J. Ma, H. Bin Yang, H. Xiao, J. Li, Y. Xiong, Y. Huang, B. Liu, Selective photoelectrochemical oxidation of glycerol to high value-added dihydroxyacetone, Nat. Commun. 10 (2019) 1779, https://doi.org/10.1038/s41467-019-09788-5.
[40] J. De Paula, D. Nascimento, J.J. Linares, Influence of the anolyte feed conditions on the performance of an alkaline glycerol electroreforming reactor, J. Appl. Electrochem. 45 (2015) 689–700, https://doi.org/10.1007/s10800-015-0848-6.
[41] G. Wang, J. Chen, K. Li, J. Huang, Y. Huang, Y. Liu, X. Hu, B. Zhao, L. Yi, T. W. Jones, Z. Wen, Cost-effective and durable electrocatalysts for Co-electrolysis of CO_2 conversion and glycerol upgrading, Nano Energy 92 (2022), 106751, https://doi.org/10.1016/J.NANOEN.2021.106751.
[42] M.A. Khan, S.K. Nabil, T. Al-Attas, N.G. Yasri, S. Roy, M.M. Rahman, S. Larter, P. M. Ajayan, J. Hu, M.G. Kibria, Zero-crossover electrochemical CO_2 reduction to ethylene with co-production of valuable chemicals, Chem Catal. 2 (2022) 2077–2095, https://doi.org/10.1016/J.CHECAT.2022.06.018.
[43] X. Han, H. Sheng, C. Yu, T.W. Walker, G.W. Huber, J. Qiu, S. Jin, Electrocatalytic oxidation of glycerol to formic acid by $CuCo_2O_4$ spinel oxide nanostructure catalysts, ACS Catal. 10 (2020) 6741–6752, https://doi.org/10.1021/acscatal.0c01498.
[44] M.B.C. De Souza, R.A. Vicente, V.Y. Yukuhiro, C.T.G. Pires, W. Cheuquepán, J. L. Bott-Neto, J. Solla-Gullón, P.S. Fernández, Bi-modified Pt electrodes toward glycerol electrooxidation in alkaline solution: effects on activity and selectivity, ACS Catal. 9 (2019) 5104–5110, https://doi.org/10.1021/acscatal.9b00190.
[45] C.C. Lima, M.V.F. Rodrigues, A.F.M. Neto, C.R. Zanata, C.T.G Vilela Menegaz Teixeira Pires, L.S. Costa, J. Solla-Gullón, P.S. Fernández, Highly active Ag/C nanoparticles containing ultra-low quantities of sub-surface Pt for the electrooxidation of glycerol in alkaline media, Appl. Catal. B Environ. 279 (2020), 119369, https://doi.org/10.1016/J.APCATB.2020.119369.
[46] X. Guo, S.-M. Xu, H. Zhou, Y. Ren, R. Ge, M. Xu, L. Zheng, X. Kong, M. Shao, Z. Li, H. Duan, Engineering hydrogen generation sites to promote electrocatalytic CO_2 reduction to formate, ACS Catal. 12 (2022) 10551–10559, https://doi.org/10.1021/acscatal.2c02548.
[47] B. van den Bosch, B. Rawls, M.B. Brands, C. Koopman, M.F. Phillips, M. C. Figueiredo, G.J.M. Gruter, Formate over-oxidation limits industrialization of glycerol oxidation paired with carbon dioxide reduction to formate, ChemPlusChem 88 (2023), e202300112, https://doi.org/10.1002/cplu.202300112.
[48] A.J.R.C. Junqueira, D. Das, A.C. Brix, S. Dieckhöfer, J. Weidner, X. Wang, J. Shi, Simultaneous anodic and cathodic formate production in a paired electrolyzer by CO_2 reduction and glycerol oxidation, ChemSusChem 16 (2023), e202202349, https://doi.org/10.1002/cssc.202202349.
[49] J. Vehrenberg, J. Baessler, A. Decker, R. Keller, Paired Electrochemical synthesis of formate via oxidation of glycerol and reduction of CO_2 in a flow cell reactor, Electrochem. Commun. (2023), 107497, https://doi.org/10.1016/j.elecom.2023.107497.
[50] T. Andreu, M. Mallafré, M. Molera, M. Sarret, R. Oriol, I. Sirés, Effect of thermal treatment on nickel-cobalt electrocatalysts for glycerol oxidation, ChemElectroChem 9 (2022) 1–7, https://doi.org/10.1002/celc.202200100.
[51] G. Díaz-Sainz, M. Alvarez-Guerra, J. Solla-Gullón, L. García-Cruz, V. Montiel, A. Irabien, CO_2 electroreduction to formate: continuous single-pass operation in a filter-press reactor at high current densities using Bi gas diffusion electrodes, J. CO_2 Util. 34 (2019) 12–19, https://doi.org/10.1016/j.jcou.2019.05.035.
[52] G. Díaz-Sainz, K. Fernández-Caso, T. Lagarteira, S. Delgado, M. Alvarez-Guerra, A. Mendes, A. Irabien, Coupling continuous CO_2 electroreduction to formate with efficient Ni-based anodes, J. Environ. Chem. Eng. 11 (2023), 109171, https://doi.org/10.1016/J.JECE.2022.109171.
[53] H. Wan, C. Dai, L. Jin, S. Luo, F. Meng, G. Chen, Y. Duan, C. Liu, Q. Xu, J. Lu, Z. J. Xu, Electro-oxidation of glycerol to high-value-added C1–C3 products by iron-substituted spinel zinc cobalt oxides, ACS Appl. Mater. Interfaces. 14 (2022) 14293–14301, https://doi.org/10.1021/acsami.2c02215.
[54] X. Huang, Y. Zou, J. Jiang, Electrochemical oxidation of glycerol to dihydroxyacetone in borate buffer: enhancing activity and selectivity by borate−polyol coordination chemistry, ACS Sustain. Chem. Eng. 9 (2021) 14470–14479, https://doi.org/10.1021/acssuschemeng.1c04795.
[55] M. Batista Cordeiro Souza, Development of p-block adatom-modified platinum electrocatalysts for the electrochemical conversion of glycerol in alkaline medium, University of Campinas, Sao Paulo, 2022. PhD Thesis.
[56] M. Pérez-fortes, E. Tzimas, Techno-economic and environmental evaluation of CO_2 utilsation for fuel production. Synthesis of methanol and formic acid., Publications Office of the European Union, Luxemburg, 2016. https://doi.org/10.2790/89238.
[57] E. Irtem, T. Andreu, A. Parra, M.D. Hernández-Alonso, S. García-Rodríguez, J. M. Riesco-García, G. Penelas-Pérez, J.R. Morante, Low-energy formate production from CO_2 electroreduction using electrodeposited tin on GDE, J. Mater. Chem. A. 4 (2016) 13582–13588, https://doi.org/10.1039/c6ta04432h.